Coating 3D Printed Polycaprolactone Scaffolds with Nanocellulose Promotes Growth and Differentiation of Mesenchymal Stem Cells

Ahmad Rashad[a*], Samih Mohamed-Ahmed[a], Miina Ojansivu[a,b], Kaia Berstad[a] , Mohammed A. Yassin[a,c], Tove Kivijärvi[c], Ellinor Bævre Heggset[d], Kristin Syverud[d,e], Kamal Mustafa[a*]

[a]Department of Clinical Dentistry, University of Bergen, Bergen, Norway.

[b]Adult Stem Cell Research Group, Faculty of Medicine and Life Sciences and BioMediTech Institute, University of Tampere, Tampere, Finland.

[c]Department of Fiber and Polymer Technology, Royal Institute of Technology (KTH), Stockholm, Sweden.

[d]RISE PFI, Trondheim, Norway.

[e]Department of Chemical Engineering, Norwegian University of Science and Technology (NTNU), Trondheim, Norway.

[*]Corresponding authors:

Kamal Mustafa, Ph.D.

E-mail: Kamal.Mustafa@uib.no

Ahmad Rashad, Ph.D.

E-mail: ahmad.elsebahy@uib.no

Department of Clinical Dentistry, University of Bergen, Norway

Phone: +4755586097

KEYWORDS:

Cellulose Nanofibrils, 3D printing, Wettability, Osteogenic differentiation

Abstract

3D printed polycaprolactone (PCL) has potential as a scaffold for bone tissue engineering, but the hydrophobic surface may hinder optimal cell responses. The surface properties can be improved by coating the scaffold with cellulose nanofibrils material (CNF), a multiscale hydrophilic biocompatible biomaterial derived from wood. In this study, human bone marrow-derived mesenchymal stem cells were cultured on tissue culture plates (TCP) and 3D printed PCL scaffolds coated with CNF. Cellular responses to the surfaces (viability, attachment, proliferation and osteogenic differentiation) were documented. CNF significantly enhanced the hydrophilic properties of PCL scaffolds and promoted protein adsorption. Live/dead staining and lactate dehydrogenase release assays confirmed that CNF did not inhibit cellular viability. The CNF between the 3D printed PCL strands and pores acted as a hydrophilic barrier, enhancing cell seeding efficiency and proliferation. CNF supported the formation of a well-organized actin cytoskeleton and cellular production of vinculin protein on the surfaces of TCP and PCL scaffolds. Moreover, CNF-coated surfaces enhanced not only alkaline phosphatase activity, but also collagen Type-I and mineral formation. It is concluded that CNF coating enhances cell attachment, proliferation and osteogenic differentiation and has the potential to improve the performance of 3D printed PCL scaffolds for bone tissue engineering.

Introduction

In nature, extracellular matrix (ECM) has hierarchical topographical features ranging in scale from micrometer to nanometer.[1] This hierarchical architecture directs cell behavior by providing spatiotemporal cues to guide cellular functions.[2] To fabricate biomimetic scaffolds, the complex physicochemical properties of the ECM must be considered. However, incorporating complex parameters into a synthetic scaffold is difficult and requires advanced manufacturing techniques.[3] Unlike conventional processing methods, which remove material in a subtractive manner, the principle of the three-dimensional (3D) printing method is to fabricate objects by adding material layer by layer.[4, 5] 3D printed scaffolds are increasingly being applied in tissue engineering because of the precise control of the porosity and geometry of the structures.[5, 6] Moreover, patient-specific customization by fabricating personalized scaffolds from computed tomography images facilitated the clinical applications of tissue engineering.[7]

Among different biomaterials, 3D printed polycaprolactone (PCL) has been tested widely for both soft and hard tissue engineering applications.[8-10] PCL is approved by the US Food and Drug Administration (FDA) and has good biocompatibility and mechanical strength.[11, 12] Moreover, the low melting point makes it an ideal thermoplastic polymer for 3D printing applications.[13] However, PCL is hydrophobic and lacks an active surface for optimal cell responses.[14] Several surface modifications have therefore been introduced to enhance cell-PCL interactions.[13, 15, 16] Alkaline hydrolysis with sodium hydroxide (NaOH) for instance, was shown to alter the surface chemistry, increase the hydrophilicity of PCL scaffolds and enhance cellular activity.[14] Plasma treatments have been used also to change the surface chemistry and topography without changing the bulk properties of the scaffold.[15] Coating the surface of 3D printed PCL scaffolds with collagen nanofibers was also found to improve biological activity.[17, 18] Collagen is

the most abundant fibrous hierarchical protein in bone ECM and contains amino acidic sequences for cell attachment.[1] The major disadvantages include the high cost of manufacturing and the complex procedures required for purification.[19]

In analogy with collagen, cellulose is the main building block of wood and other plants.[20] Nanocellulose biomaterials are polysaccharide biopolymers which can be produced by bacteria (bacterial nanocellulose; BNC) or extracted from plants (cellulose nanofibrils; CNF) by mechanical treatment and chemical oxidation using 2,2,6,6-tetramethylpiperidine-1-oxyl radical (TEMPO).[21, 22] Of immunological importance, CNF, unlike collagen and bacterial cellulose, is not of microbial or animal origin.[23] As a nanoscale material, wood-based nanocellulose have remarkable physicochemical properties, including a high specific surface area, surface reactivity and good mechanical properties.[20] Because of their biocompatibility, CNF hydrogels have recently been used in various tissue engineering applications, such as human pluripotent stem cell culture, differentiation of human hepatic cells and human chondrocyte bio-printing.[24-27] However, the application of CNF in bone tissue engineering has yet to be reported: to date there are no enough published studies of the effect on surface properties of coating 3D printed PCL bone scaffolds with CNF. The aim of the present study was therefore to develop a TEMPO-oxidized CNF coating on 3D printed PCL scaffolds for bone tissue engineering applications. To study the influence of CNF alone on the basic responses of hBMSCs, nanocellulose was first coated on tissue culture plates (TCP) and cell viability, attachment, proliferation and differentiation were evaluated. In the next phase, 3D printed PCL scaffolds were etched with NaOH and coated with CNF, in an attempt to improve the surface properties. The modified scaffolds were evaluated for roughness, wettability and protein adsorption as well as for attachment, proliferation and differentiation of hBMSCs. A schematic illustration of the study design is shown in Fig. 1.

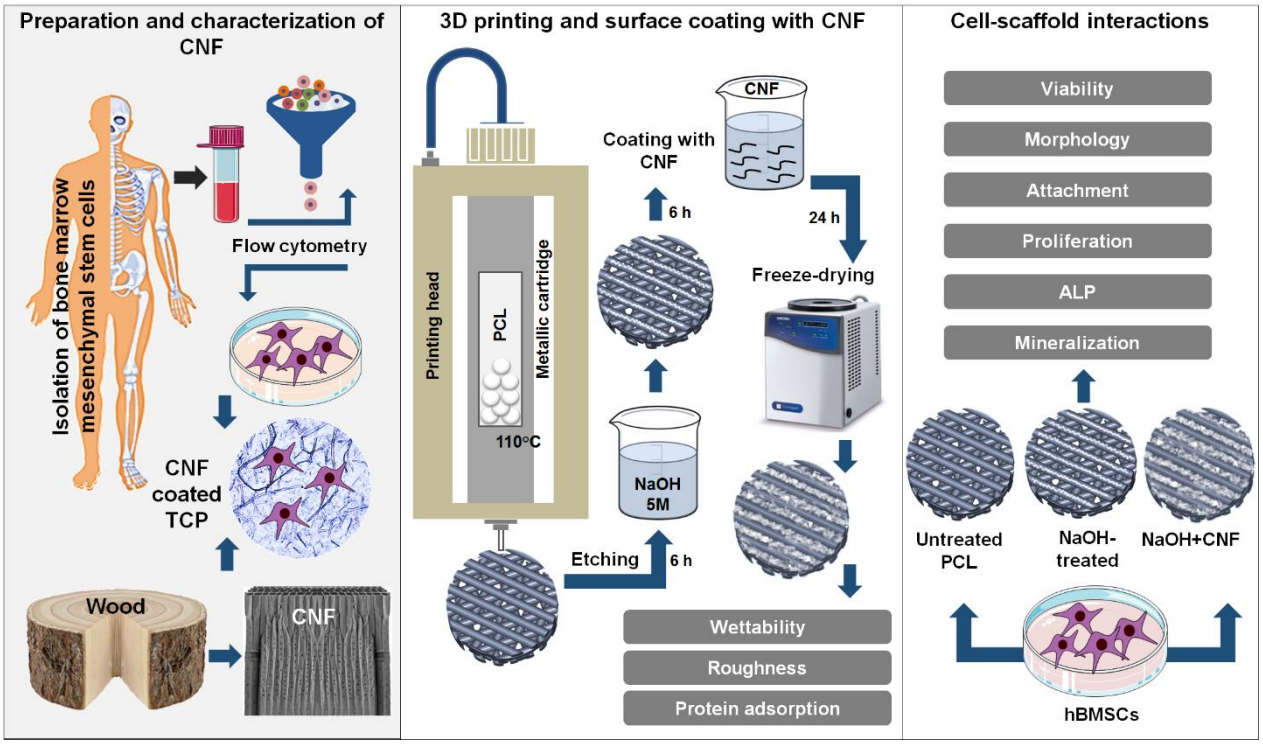

Figure 1. Schematic illustration of the study design. After preparation and characterization of CNF, hBMSCs were isolated, characterized and cultured on CNF-coated tissue culture plates (TCP) or 3D printed PCL scaffolds after etching with NaOH.

Materials and Methods

Preparation and characterization of CNF

Fully bleached, never-dried softwood kraft pulp was kindly donated by Södra Cell (Växjö, Sweden). Nanocellulose was produced by chemical and mechanical treatments, according to a previously described method[22]. Briefly, 2,2,6,6-tetramethylpiperidinyl-1-oxyl (TEMPO) (Sigma-Aldrich, MO, USA) was used to catalyze the oxidation of the alcohol groups, using sodium bromide (NaBr). The oxidized kraft pulp (1 % consistency) was then homogenized at 1000 bar pressure (APV, SPX Flow Technology, Silkeborg, Denmark). The content of the carboxyl and aldehyde groups was determined by conductometric titration using an automatic titrator (Metrohm 902

Titrando). This analysis was repeated after oxidation of aldehyde groups to carboxyl groups with $NaClO_2$. The aldehyde content was calculated from the difference in carboxylate content before and after the oxidation. To evaluate the structure of the prepared CNF, glass coverslips were coated with CNF suspension and incubated at 37°C overnight to evaporate the water. Surfaces were analyzed by optical microscopy (Nikon Eclipse Ti, Tokyo, Japan), field emission scanning electron microscopy (SEM; JEOL JSM-7400F, Tokyo, Japan) and atomic force microscopy (diMultiMode V AFM, Bruker, USA).

3D printing and surface modifications of PCL scaffolds

PCL (MW 45 kDa, melting temperature = 60°C, Sigma-Aldrich) pellets were melted at 110°C in a metallic cartridge of 3D-Bioplotter (EnvisionTEC, Gladbeck, Germany) and extruded through a needle with an inner diameter of 400 µm. Square-shaped scaffolds measuring 30 mm×30 mm, composed of four layers with an orientation of 0°-45°-90°-135° and strand spacing of 1mm were 3D printed and then punched to fit into 48-well plates. The scaffolds were cleansed with 70% ethanol for 15 min, etched with 5M NaOH (Sigma-Aldrich) for 6 h and then washed with deionized H_2O until the pH reached 7.4. After etching, the scaffolds were immersed in CNF solution (0.33% solid content) for 6 h and then freeze-dried for 24 h. To confirm that NaOH etching has no negative effect on the bulk properties of the 3D printed scaffolds, tensile testing was performed on printed unmodified and NaOH-etched, four-layered dumbbell-shaped samples at room temperature, using a material testing system (MTS 858 MiniBionix II, USA) at a stretching speed of 0.5 mm/s.

Structural and surface characterization of the scaffolds

Stereomicroscopic (Leica M205C, Heerbrugg, Switzerland) images were taken for 2D morphological characterization of the printed scaffolds. For 3D assessment of the morphology, porosity and surface area, 3D volume rendered images were obtained with a micro-CT scanner

(Skyscan 1172VR, Kontich, Belgium). To investigate the effect of the surface treatment on the roughness, SEM images were acquired before and after modifications. To study the effect of the surface modifications on the wettability of the scaffolds, the contact angle was measured with a KSV CAM Contact Angle and Surface Tension Meter (KSV Instruments, Finland) with a 3 µL drop of deionized water. To confirm the stability of the CNF on the printed scaffolds, samples were stored at room temperature (RT) for 3 months followed by soaking in cell culture medium at 37°C for 7 days. Stereomicroscope and SEM were used to characterize the stored samples.

Water uptake

Dried scaffolds were initially weighed and then immersed in distilled water colored with crystal violet blue dye (Merck, Darmstadt, Germany). After 30 minutes, the scaffolds were weighed after wiping off the excess surface water. The water uptake (%) was calculated as follows:

$$\text{Water uptake (\%)} = \frac{(\text{Weight}_{30\text{min}} - \text{Weight}_0)}{\text{Weight}_0} x\ 100$$

Total protein adsorption

The scaffolds were incubated in Dulbecco's modified Eagle's medium (DMEM) (Life Technologies, Gibco, Carlsbad, CA, USA) with 10% fetal bovine serum (FBS) (HyClone, GE Healthcare, Utah, USA) at 37°C for 24 h. The scaffolds were then washed with Dulbecco's phosphate buffered saline (PBS) (Life Technologies) to remove weakly adsorbed proteins and incubated in 2% sodium dodecyl sulfate (Sigma-Aldrich) for 20 h. The total amount of protein was measured by a commercial protein assay kit (Pierce ™BCA Protein Assay, Rockford, IL, USA) according to manufacturer's instructions.

Isolation and characterization of hBMSCs

After obtaining patient consent and approval from the Regional Committee for Medical and Health Research Ethics (REK) in Norway (2013/1248/REK), hBMSCs were isolated from two young patients at the Department of Plastic Surgery, Haukeland University Hospital, Bergen, Norway. Briefly, the bone marrow aspirate was filtered through a cell strainer and diluted in DMEM growth culture medium supplemented with 10% FBS and 1% antibiotics (100 U/ml penicillin and 0.1 mg/ml streptomycin) (GE Healthcare). After centrifugation, the resulting pellet was suspended in growth culture medium and plated in a 75 cm^2 culture flask at 37°C in 5% CO_2. After 24 h, the cells were washed with PBS and fresh culture medium was added. For characterization of the mesenchymal origin, flow cytometry was used with the following stem cell markers: CD34, CD45, CD73, CD90, CD105 and HLA-DR (BD Biosciences, San Jose, CA, USA).[28] Cells from passages 4-6 were used in the experiments.

Cell seeding

To evaluate cellular responses to CNF, hBMSCs were grown on CNF coated 24-well plates. Viability, attachment, morphology, proliferation and osteogenic differentiation were assessed. A volume of 400 µl of CNF suspension (0.33% solid content) was used to cover each well and then incubated at 37°C to evaporate the water. Uncoated tissue culture polystyrene plates (TCP) were used as controls. The cell density was 1.5×10^4 cells/well. To evaluate the cellular response on the 3D printed scaffolds, three groups were used in this study: unmodified PCL, NaOH-etched PCL and PCL coated with CNF after etching (CNF+NaOH). Unless otherwise stated, cells (2×10^5/ scaffold) were seeded onto the different scaffolds in 48-well plates. The seeded scaffolds were cultured in DMEM medium supplemented with β-glycerophosphate disodium salt hydrate, ascorbic acid and dexamethasone (Sigma-Aldrich). In all experiments fresh medium was supplied twice a week.

Cell viability, morphology and proliferation on CNF coated surfaces

The viability of the cells cultured on CNF-coated TCP at 1 and 4 days was analyzed by live/dead staining (Invitrogen, Life Technologies). Cells were incubated in a working solution containing EthD-1 (stains dead cells red) and Calcein-AM (stains living cells green) for 30 min and then imaged with a fluorescence microscope (Nikon Eclipse Ti, Tokyo, Japan). Cells cultured on the 3D printed scaffolds were stained after 21 days. To evaluate the toxicity of CNF, lactate dehydrogenase (LDH) release was measured using a colorimetric kit (Abcam, Cambridge, UK). The medium corresponding to the live/dead assay was collected after 1 and 4 days and centrifuged at 10000 × g at 4°C. The enzymatic assay was conducted in accordance with the manufacturer's instructions.

To study the morphological changes, the cells cultured on CNF-coated TCP were fixed with 4% paraformaldehyde after 24h and incubated in a solution of phalloidin-Atto488/PBS (Sigma-Aldrich) (dilution 1:50) for 45 min at room temperature, protected from light. The cells were then imaged with a fluorescence microscope. After 4 hours, cells cultured on 3D printed scaffolds were stained with phalloidin according to the above-described protocol.

Cell proliferation was evaluated using a CyQUANT cell proliferation assay kit (Invitrogen, Life Technologies). Briefly, after 3 and 10 days of culture in osteogenic medium, cells grown on CNF-coated TCP and 3D printed scaffolds were lysed with 0.1% Triton-X100 buffer before freezing (-80°C). Samples were then subjected to two freeze-thaw cycles and sonicated for 60 seconds. In 96-well plates, parallel samples of each lysate (20 µl) were mixed with 180 µl of working solution containing CyQUANT GR dye and cell lysis buffer. The fluorescence at 480/520 nm was measured with a microplate reader (FLUOstar OPTIMA, BMG LABTECH, Germany).

Cell seeding efficiency and attachment on CNF-coated 3D printed scaffolds

Cells (5×10^5) were seeded on the 3D printed scaffolds, allowed to attach for 2 h and then covered with medium. After a further 2 h, the scaffolds were transferred to new wells and cells attached to the bottom of the wells (unattached to the scaffold) were trypsinized and quantified using an automated cell counter (Countness™, Invitrogen, CA, USA). Cell seeding efficiency was quantified as described below:

$$\text{Seeding efficiency (\%)} = \frac{(\text{Initial cell number} - \text{cells unattached to the scaffolds})}{\text{Initial cell number}} \text{ x } 100$$

After 4 hours and 7 days, spreading of the cells was observed by SEM after fixation with 3% glutaraldehyde. The fixed scaffolds were vacuum dried, sputter-coated with platinum and imaged at 5 kV.

Immunocytochemical staining

The production of vinculin protein after 24 h of culture and collagen Type-I after 14 and 28 days of culture on CNF-coated TCP were studied using immunocytochemical staining (ICC). Cells were fixed with 4% paraformaldehyde (15 min at RT), permeabilized in 0.1% Triton X-100 and blocked with 1% bovine serum albumin (BSA; Sigma-Aldrich). Mouse monoclonal anti-vinculin (Clone hVIN-1, V9131, Sigma-Aldrich; dilution1:400) and rabbit polyclonal anti-collage Type I (Abcam; dilution 1:500) were incubated for 2h at RT under shaking. The secondary antibodies used were; goat anti-mouse Alexa Fluor 568 IgG (dilution 1:250) and goat anti-rabbit Alexa Fluor 546 IgG (dilution 1:800) (Life Technologies). The actin cytoskeleton was stained with phalloidin-Atto488 (dilution 1:50), which was incubated simultaneously with the secondary antibodies for 45 min at RT. Finally, after washing with PBS, the nuclei were stained with 4´,6-diamidino-2-phenylindole (DAPI) (Sigma-Aldrich) (dilution 1:2000). The samples were imaged with a Nikon inverted fluorescent microscope. Stained samples without cells were used as blanks and samples with only

secondary antibody treatment were used as negative controls to confirm that the CNF has no background staining.

Western blot analysis

The amount of vinculin produced by the cells cultured on CNF-coated plates or the 3D printed scaffolds after 24 h was determined by Western blot analysis. Cells were lysed directly into 2x Laemmli sample buffer (Bio-Rad, CA, USA). The proteins in the samples were then separated with SDS-PAGE (sodium dodecyl sulfate polyacrylamide gel electrophoresis). The proteins were transferred to a polyvinylidene fluoride membrane (PVDF; GE Healthcare, UK). Non-fat milk was used as a blocking solution. The target proteins were then probed with the following primary antibodies: mouse monoclonal anti-β-actin (Santa Cruz Biotechnology; Dallas, Texas USA; dilution 1:2000) and vinculin ABfinity^{TM} recombinant rabbit antibody (Life Technologies; dilution 1:2000). The HRP-conjugated secondary antibodies used were goat anti-mouse IgG and goat anti-rabbit IgG (Santa Cruz Biotechnology, dilution 1:2000). Target proteins were detected with chemiluminescence reagent (ECL; GE Healthcare) using the ChemiDoc MP imaging system (Bio-Rad, CA, USA).

Alkaline phosphatase activity

ALP activity after 3 and 10 days of culture in osteogenic medium was analyzed from the same Triton-X 100 lysates used in the proliferation test. Briefly, 90 µl of working solution containing 1:1 Sigma 104® phosphatase substrate and alkaline buffer solution (Sigma-Aldrich) was added to 20µl of each sample lysate in 96-well plates and incubated for 20 min at 37°C. After incubation, 50 µl of 1M NaOH was added to the wells to stop the reaction. Absorbance was measured at 405 nm. The results were normalized to the cell number determined by the proliferation test.

Mineralization

Calcium deposition was assessed by Alizarin red S staining. Briefly, cells on CNF-coated TCP after 28 days and on 3D printed scaffolds after 21 days were fixed with 4% paraformaldehyde for 1 h and stained with 2% Alizarin red (Sigma-Aldrich) solution (pH 4.1) for 15 min at RT. After washing and air-drying, images were taken with an optical microscope (Nikon, Tokyo, Japan). For quantification, the color was extracted with 100 mM cetylpyridinium chloride (Sigma-Aldrich) and the absorbance was measured at 540 nm. Cell-free samples were stained to act as blank samples.

Statistical analysis

Statistical analysis was performed using One-way ANOVA with a Tukey's post-hoc comparison of the mean using SPSS software (IBM, Armonk, NY, USA). Data are expressed as the mean ± standard deviation (SD). Differences were considered statistically significant at $p \leq 0.05$.

Results

Preparation and characterization of CNF

The prepared TEMPO-oxidized CNF material had a gel-like consistency with solid content of 1.06 ± 0.01. Structural investigation by different imaging methods showed that the CNF has a hierarchical multiscale fibrillary structure, ranging in scale from several micrometers to nanometers (Figure 2). Conductometric titration disclosed that as well as the hydroxyl groups, the samples contained aldehyde (211 ± 60 µmol/g) and carboxyl (764 ± 60 µmol/g) surface groups.

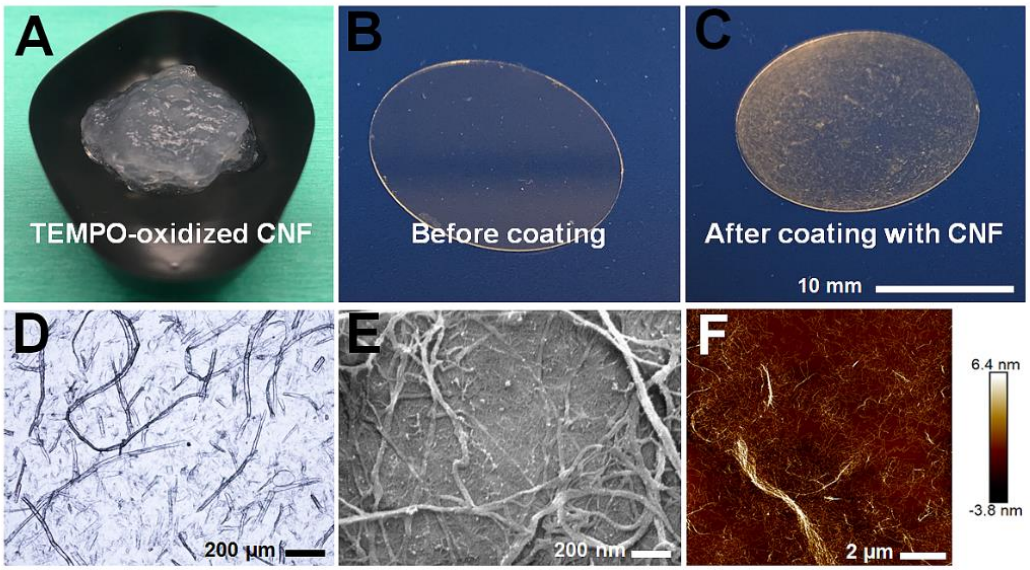

Figure 2. Structural characterization of the prepared CNF showing the multiscale fibrillary nature. (A) Macroscopic image of the prepared hydrogel-like CNF. (B) Glass coverslips before and (C) after coating with CNF. (D) Optical microscope image showing microscale fibers. (E) SEM and (F) AFM images showing nanoscale fibrils (6.4 nm).

3D printing and surface treatment of PCL scaffolds

The stereomicroscopic images revealed that the printed scaffolds had 1 mm strand spacing and strand orientation of 0°-45°-90°-135° (Figure 3A). To assess the effect of the etching on the mechanical properties of the scaffolds, tensile strength testing was conducted on the untreated control and NaOH-treated PCL scaffolds. Statistical analysis disclosed no significant inter-group differences in the tensile strength or the moduli (Figure S1). The micro-CT images showed that the internal structure of the scaffolds comprised complex polygonal geometries with fully interconnected porosity. Surface area and porosity were quantified from the micro-CT images of the scaffolds (Figure S2). The percentage porosity of untreated PCL, NaOH treated and CNF coated samples were 37.6 ± 3.3, 38.8 ±1.1 and 40.7 ± 1.2%, respectively. The NaOH etching and CNF coating slightly increased the surface area of the scaffolds compared with the control PCL

scaffolds. Moreover, the micro-CT and stereomicroscopic images showed that CNF was clearly located in the pores and between the layers of the scaffolds (Figure 3B and S2). In addition, cross sectional analysis of a larger CNF-coated scaffold (15 layers) showed the presence of CNF in the center of the scaffold (Figure S3). Moreover, stereomicroscopic and SEM images confirmed the stability of CNF coat on the PCL surface after 3 months at room temperature and after 7 days of incubation in cell culture medium at 37°C (Figure S4). The SEM micrographs also revealed the difference in the topography of the PCL surfaces after the surface treatments. Compared with the smooth flat surface of the control PCL, NaOH etching induced micrometer pits and holes with nanoscale roughness, while the CNF coating introduced micro-nanoscale roughness (Figure 3C).

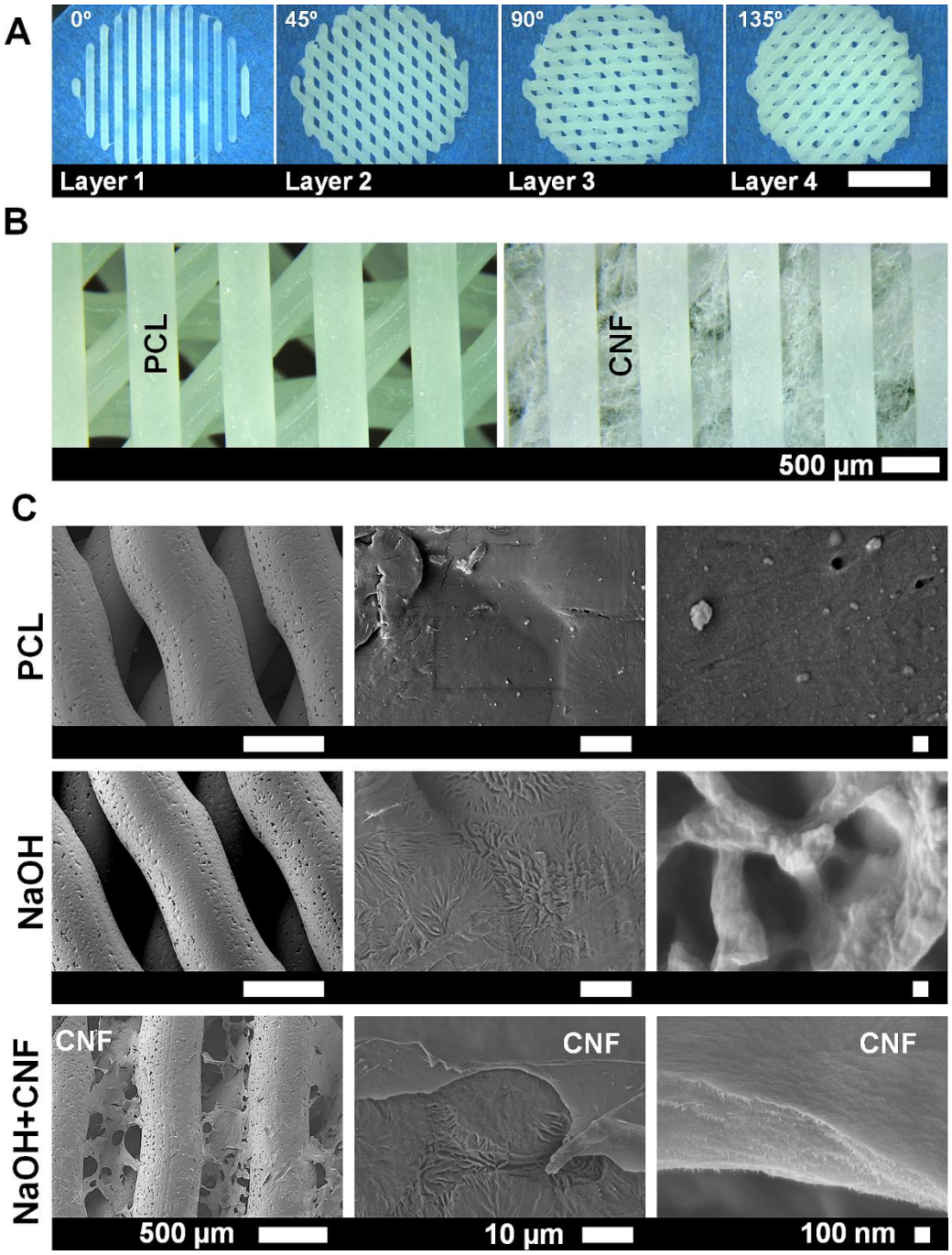

Figure 3. Structural characterization of the 3D printed PCL scaffolds. (A) Stereomicroscope images of the printed four layers with orientations of 0°-45°-90°-135° and strand spacing of 1mm (Scale bar: 5mm). (B) Stereomicroscope images of the 3D printed PCL before and after coating with CNF,

showing the cellulose fibers between the PCL strands. (C) SEM images showing the topographical changes to the PCL surface after NaOH etching and CNF coating.

Wettability and protein adsorption

To examine the hydrophilic properties of the printed scaffolds, the contact angle and water adsorption were measured (Figure 4). The contact angle of the PCL before surface treatment was 78.9° ± 3.3 and decreased to 31.4° ± 5.1 after NaOH treatment. The CNF-coated surfaces showed a contact angle of 23.5° ± 3.3. Consequently, the unmodified PCL scaffolds showed poor water uptake after 30 min (Figure 4B). Generally, water adsorption by the CNF-coated scaffolds was 3- and 2-fold greater than the control and NaOH-treated scaffolds, respectively. Similarly, the NaOH-treated scaffolds showed improved protein adsorption but compared with the untreated PCL, the difference was not significant (Figure 4C). In contrast, protein adsorption on the CNF-coated scaffolds was significantly higher than in the other groups.

Cell viability, proliferation, morphology and attachment

To study the interactions of the CNF with cells, hBMSCs were isolated, characterized and cultured on CNF-coated TCP and 3D printed scaffolds. The isolated cells exhibited strong expression of the surface proteins CD73, CD90 and CD105 (≥ 99 %), but negative expression of hematopoietic markers CD34, CD45 and HLA-DR (≤ 2%), thus verifying the mesenchymal origin of the stem cells. In order to compare the viability of hBMSCs on CNF-coated surfaces, live/dead staining and LDH assay were conducted. Generally, the results demonstrated that the CNF coating maintained cell viability (Figure 5 and S5). Very few dead cells were detected on CNF-coated TCP or on control TCP after 1 and 4 days, while no dead cells were observed on the 3D printed scaffolds at day 21. The measurement of LDH release from the cells on CNF-coated TCP showed a significant reduction from day 1 to day 4, which was similar to the control group. Although there was no

significant intergroup difference in the release of LDH, at day 4 the release was slightly lower in the CNF-coated group than in the control group.

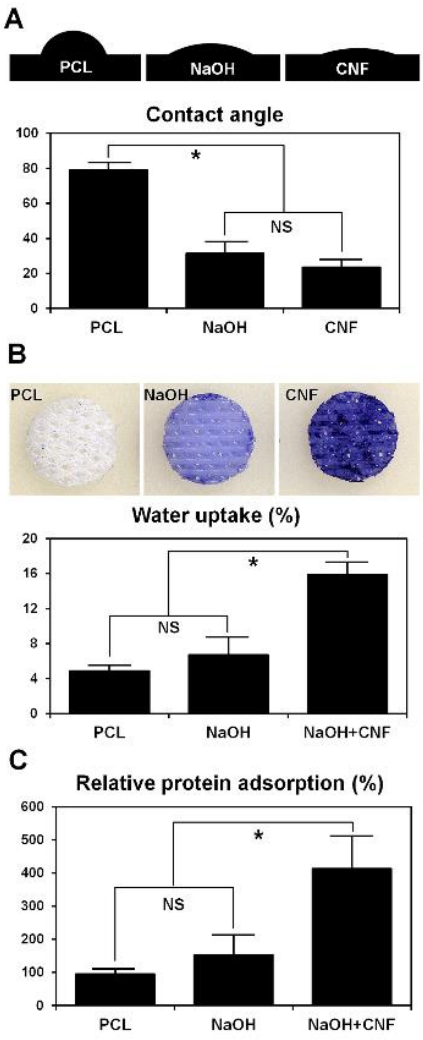

Figure 4. Surface wettability and protein adsorption. (A) Initial contact angle (*$p < 0.001$; n = 3). (B) Water uptake (*$p < 0.001$; n = 6). (C) Relative protein adsorption (*$p < 0.001$; n = 6). NS = not significant.

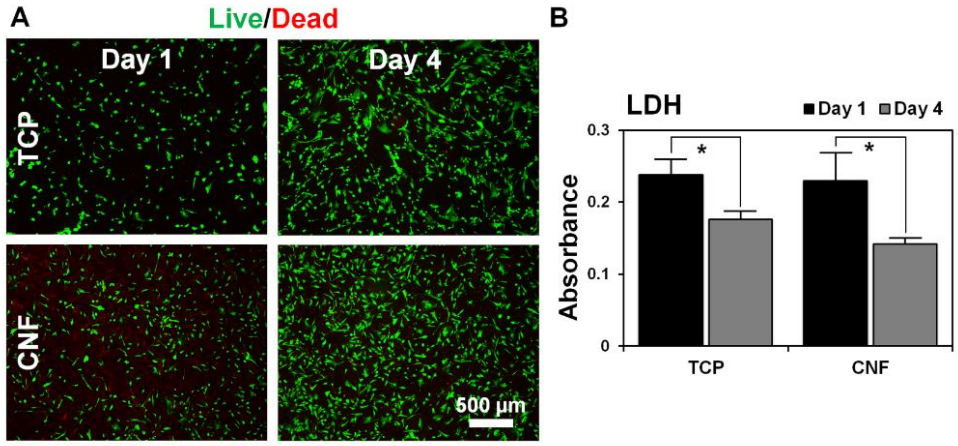

Figure 5. Cell viability and cytotoxicity on CNF-coated TCP at 1 and 4 days. (A) Cell viability by live/dead staining. (B) Cell cytotoxicity by LDH release (*$p < 0.001$; n = 5).

As presented in Figure 6A, the seeding efficiency on 3D printed scaffolds was determined after 4 h and was significantly higher for the CNF coated scaffolds than for other groups. Moreover, SEM images showed that the CNF between the printed strands also permitted cells to attach to the top layer (Figure 6B). Generally, cell proliferation increased on all the 3D printed scaffolds from day 3 to day 10. SEM images confirmed the proliferation from 4 h to day 7: at day 7 all the scaffold surfaces were covered by cell sheets (Figure 6D). The quantitative results of the cell proliferation are shown in Figure 6C. The number of cells on the CNF-coated 3D printed PCL was significantly higher than on the untreated 3D PCL scaffolds at 3 and 10 days. On the other hand, an initial decrease in the number of cells on the CNF-coated TCP was detected at day 3 (Figure 7), yet in both TCP groups the number of cells increased significantly from day 3 to day 10. After 10 days there was no significant difference between the TCP groups.

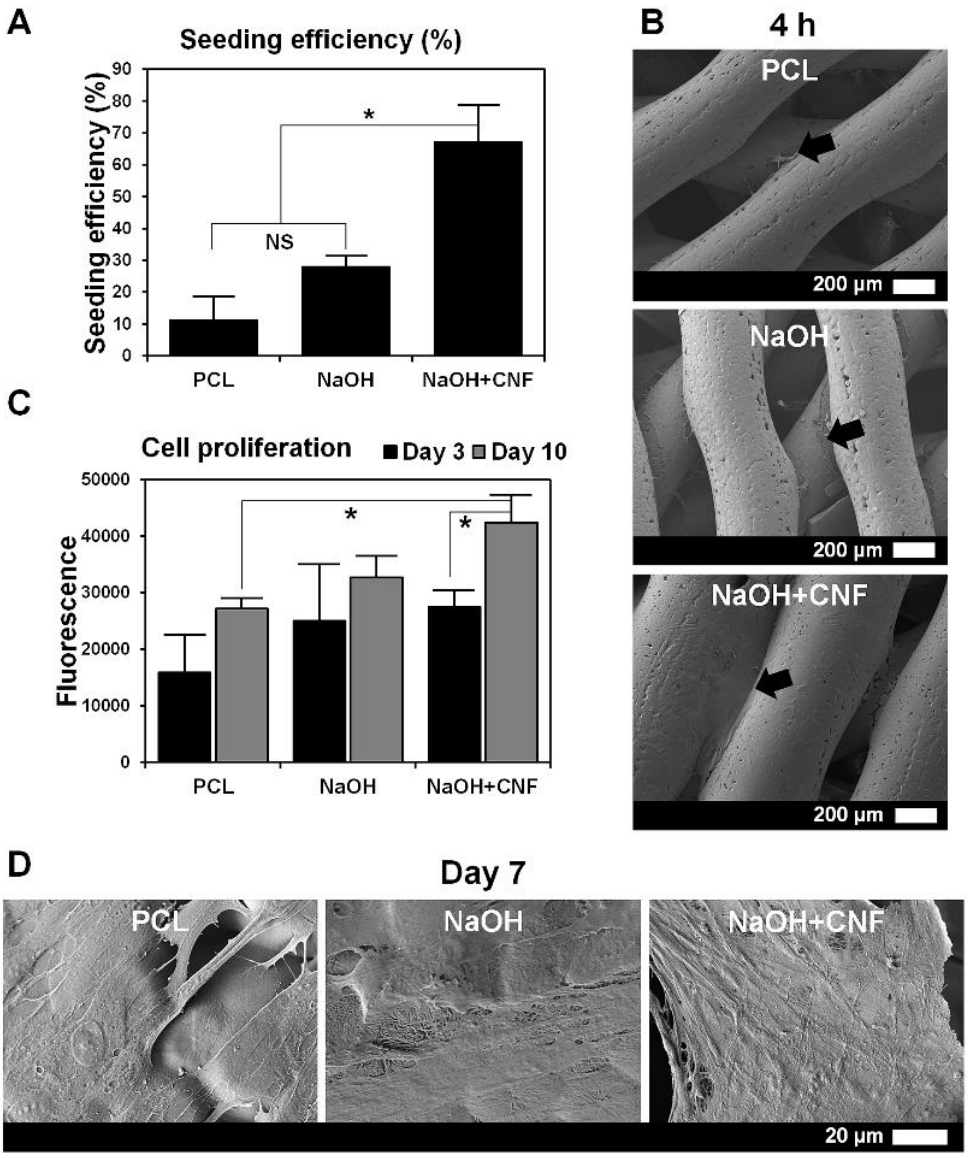

Figure 6. The influence of CNF coating on the seeding efficiency and proliferation of hBMSCs on 3D printed scaffolds. (A) Seeding efficiency after 4 h (*$p < 0.001$; n = 3). (B) SEM images of the 3D printed scaffolds showing the attached cells (arrows) on the top layer of CNF-coated scaffolds after 4 h; cells in the other groups passed to the underneath layers. (C) Proliferation of hBMSCs on the 3D printed PCL scaffolds (*$p < 0.001$; n = 5). (D) SEM images showing proliferation and spreading of the cells after 7 days.

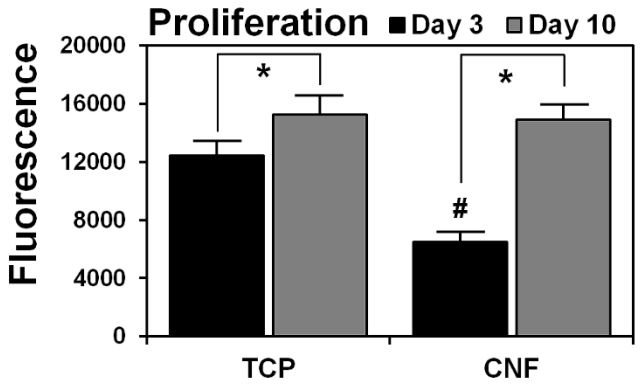

Figure 7. Proliferation of hBMSCs on CNF coated-TCP after 3 and 10 days. Significance between time points in the same group; $^{*}p < 0.001$ and between different groups; $^{\#}p < 0.001$; (n = 5).

Morphological observations of the effect of CNF on the cells were obtained from phalloidin staining of the actin cytoskeleton and SEM images. On all the TCP and PCL surfaces, the cytoskeleton was well-organized with aligned straight actin fibers inside the cells. More elongated cells were found on the CNF-coated surfaces (Figure 8 and S6). ICC and Western blotting were undertaken to evaluate the production of proteins related to cell adhesion (Figure 8). Double-staining of vinculin and actin at 24 h clearly showed production of vinculin and confirmed the elongated morphology of the cells on the CNF-coated TCP. Western blot images showed that compared to the control groups, after 24 h the CNF-coated surfaces supported comparable production of vinculin. In contrast to the relatively short filopodia on the untreated PCL, SEM micrographs at high magnification revealed that on modified PCL surfaces the cells developed filopodia to detect the surrounding environment (Figure 9).

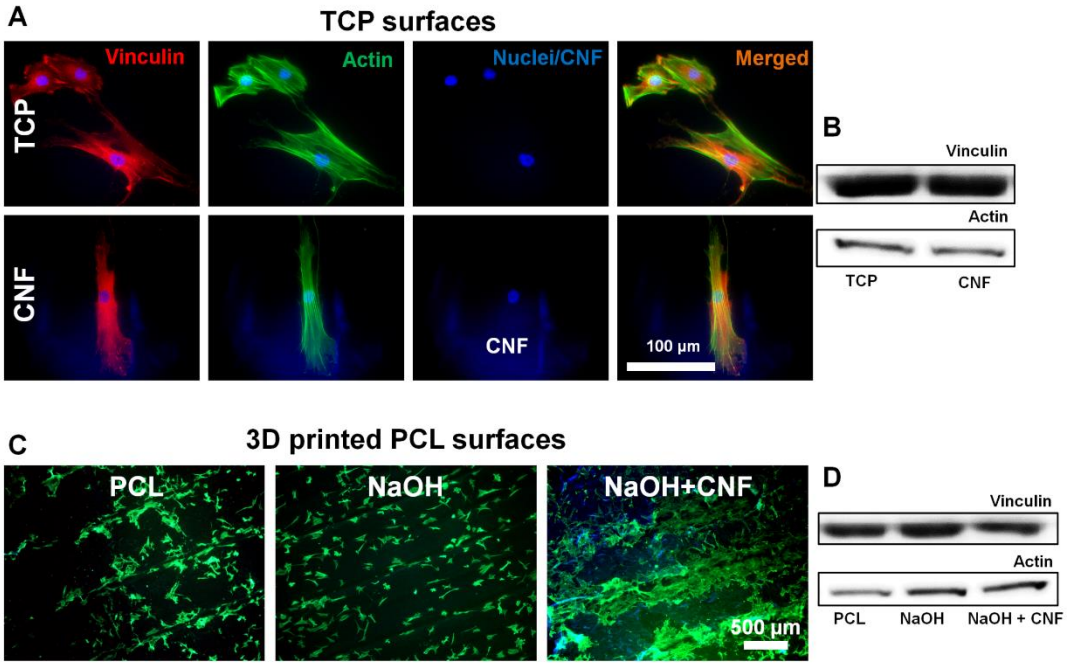

Figure 8. Cell attachment on TCP and 3D printed scaffolds (A) Immunostaining and (B) Western blot analysis showing vinculin production in cells cultured on CNF-coated TCP after 24 h. (C) Fluorescent images of cell cytoskeleton stained by phalloidin on 3D printed PCL scaffolds after 4 h. (D) Production of vinculin in cells cultured on CNF-coated 3D printed PCL after 24 h, by Western blot.

Alkaline phosphatase activity

ALP activity, an early marker of osteogenic differentiation, was analyzed to assess the osteogenic potential of the CNF-coated surfaces. After normalization to the total cell amount, ALP activity was found to be elevated in all groups from 3 to 10 days. However, this difference was statistically significant only in the CNF-coated groups. Moreover, at day 10, ALP activity was significantly higher on the CNF-coated surfaces than on the uncoated groups (Figure 10).

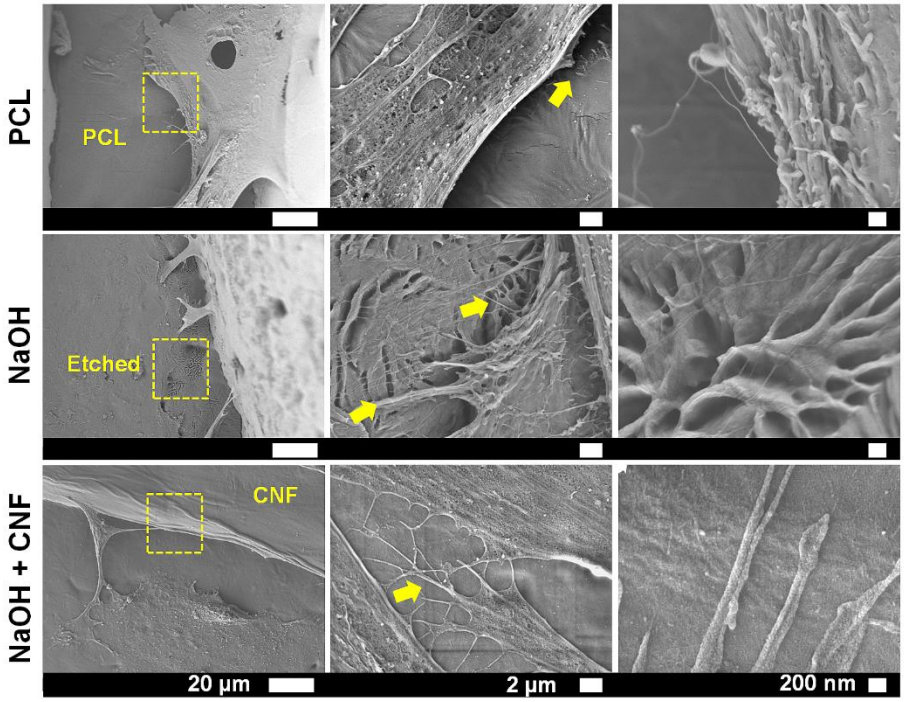

Figure 9. SEM images showing the influence of the topographical changes of the modified 3D printed PCL surfaces on the filopodia of the cells after 4 h.

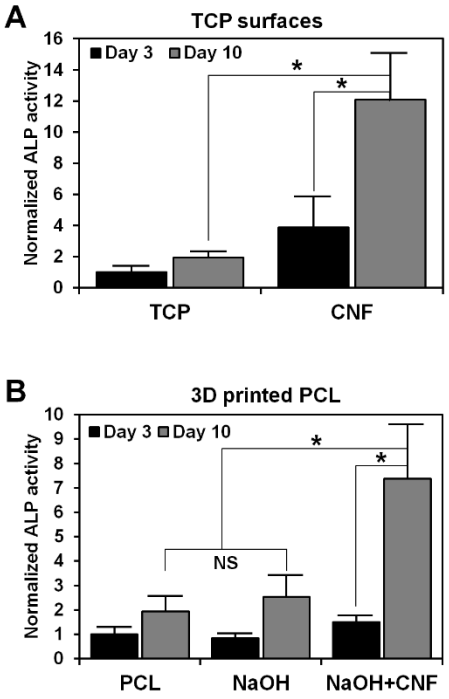

Figure 10. ALP activity after 3 and 10 days. (A) ALP activity of the cells on TCP surfaces. (B) ALP activity of the cells on 3D printed PCL before and after surface modifications. (*$p < 0.001$; n = 5).

Production of collagen Type I

After 14 days, collagen Type-I production was enhanced in the cells cultured on CNF-coated TCP compared to the control TCP (Figure 11). Moreover, collagen Type-I was clearly secreted by the cells to the ECM. However, after 28 days, the TCP groups showed similar production of collagen Type-I. The control samples confirmed that the CNF has no background staining in the collagen Type-I ICC and that the secondary antibody does not bind in unspecific ways (Figure S7).

Mineralization

In order to study the late stages of osteogenic differentiation, after 28 days TCP samples were tested by staining with Alizarin red S. As shown in Figure 12, CNF-coated TCP induced extensive mineral formation compared to the control TCP. After quantification, CNF-coated plates showed a 3-fold increase in mineralization. On the 3D PCL scaffolds, both the NaOH etching and the CNF coating enhanced the mineralization after 21 days. However, the only significant difference was between the CNF-coated PCL and the untreated PCL control group (Figure 12B). The blank samples (without cells) confirmed that the CNF does not cause background interference with the Alizarin red S stain (Figure S8).

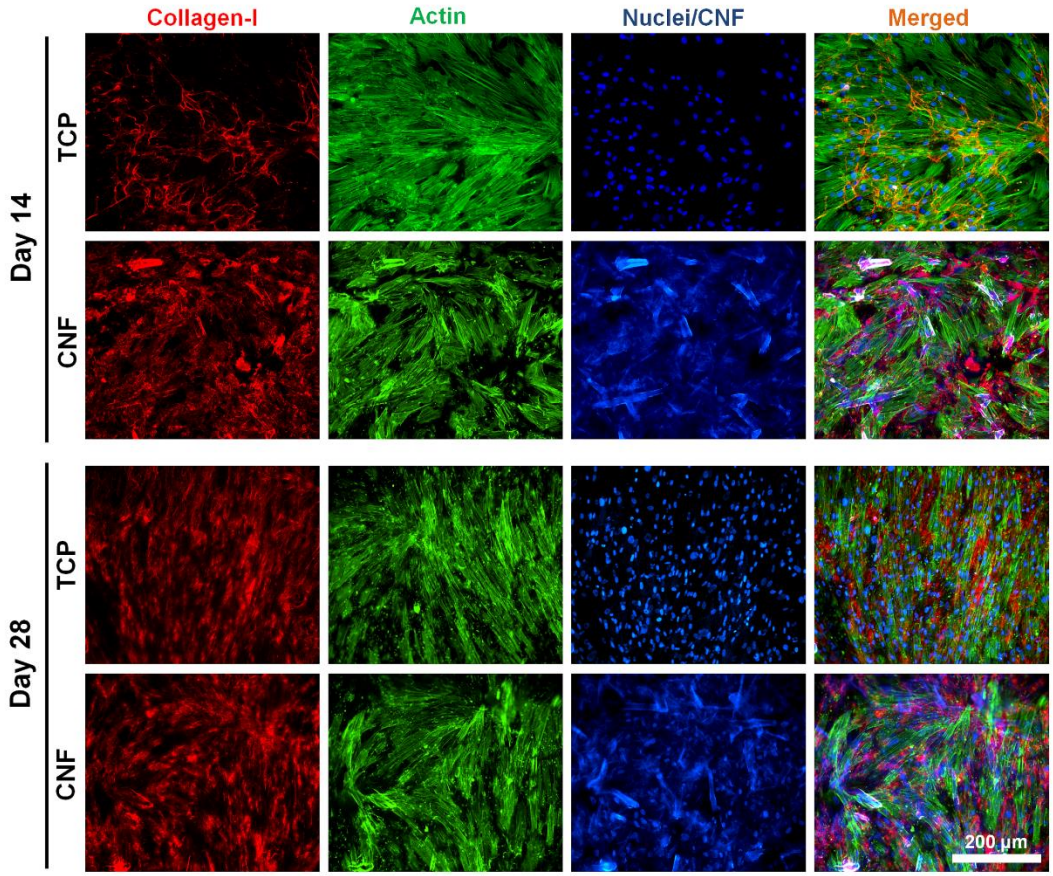

Figure 11. Collagen Type-I production and actin cytoskeleton organization of cells after 14 and 21 days.

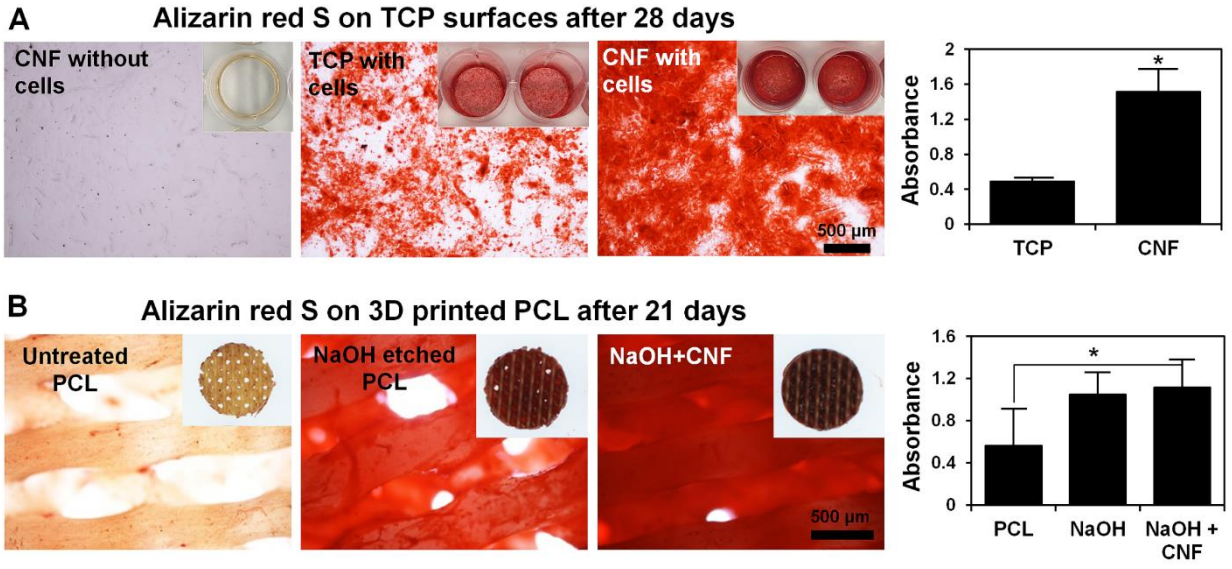

Figure 12. Mineral formation by Alizarin red S. (A) Mineralization on TCP surfaces at day 28 (*$p < 0.005$; n = 5). (B) Mineralization on 3D printed PCL scaffolds at day 21 (*$p < 0.05$; n = 5).

Discussion

The structural similarity of nanocellulose and collagen suggests that cellulose might be an appropriate material for application in the development of bone scaffolds. However, most tissue engineering studies of nanocellulose to date have been limited to the application of bacterial nanocellulose (BNC) in soft tissue regeneration.[21] There are also a limited number of reports investigating the osteogenic potential of BNC *in vitro* and *in vivo*.[29-31] In this study, it was hypothesized that coating 3D printed PCL scaffolds with CNF after NaOH etching would improve surface properties and subsequently cell behavior. To prepare the CNF material, TEMPO-oxidation was chosen because it has the ability to produce nanoscale fibrils with aldehydes and carboxyl groups on the surface.[22] For PCL scaffolds, it is known that NaOH etching improves the surface wettability of polymers by increasing surface hydrophilic groups such as carboxyl and hydroxyl groups.[32, 33] In addition to the enhanced hydrophilicity, NaOH etching is reported to introduce nanoscale roughness which improves cell adhesion.[34] Therefore, PCL surface was etched to produce hydrophilic rough surface, which would allow the CNF to be adsorbed onto the surface of the polymer. Moreover, the 0°-45°-90°-135° lay-down pattern was selected to entrap the CNF between the layers of the scaffolds. A remarkable finding was that the combination of NaOH surface treatment and CNF coating had synergistic effects: significant enhancement in surface wettability which is reported to have strong effects on protein adsorption and consequently on cell adhesion.[34] In addition, protein adsorption is strongly related to other surface properties, such as chemistry and roughness.[35, 36] McClary et al. reported that carboxyl groups not only improved protein adsorption but also supported favorable protein conformation.[37] Scopelliti et al. showed

that protein adsorption is highly dependent on surface nanostructures.[38] Jeon et al. suggested that the nanoscale features on PCL scaffolds may act as protein-binding sites.[15] Thus, the results of the present study indicate that the enhanced protein adsorption on CNF-coated scaffolds is related to the enhanced surface roughness, wettability and the presence of carboxyl and aldehyde groups on the CNF. It is likely that the aldehyde groups form a Schiff's base interaction with the amine groups of the proteins, thus facilitating the protein adsorption.[39]

As with BNC, little is known about the effect of wood-based nanocellulose on the behavior of hBMSCs. These cells were selected for the study because their high therapeutic and regenerative potential is well-established.[40] The nontoxic effect of the CNF coating was confirmed by the live/dead stain and the measurement of LDH release from the cells. With respect to cell proliferation, the reduction in cell numbers, observed after 3 days, on the CNF-coated TCP compared with the TCP control, might be due to the increased differentiation potential of hBMSCs on the CNF surface. It has been reported that hBMSCs on PCL nanofiber scaffolds proliferate slowly during the osteogenic differentiation phase.[41] Nonetheless, proliferation increased significantly from day 3 to day 10, which confirms the ability of CNF to support cell proliferation. These findings are in accordance with those of several previous studies showing that the physicochemical properties of CNF martial enable it to support cell proliferation, maintain cell viability and regulate cell spreading and morphology.[24, 42, 43]

Unlike the CNF-coated TCP, at day 3 the CNF-coated 3D printed PCL scaffolds had significantly higher numbers of cells than the control PCL scaffolds. This can be attributed to the improved cell seeding efficiency and cell attachment during the first few hours. 3D printing of biomaterials tends to produce scaffolds with interconnected open pores.[3] Cell suspensions can easily pass through these pores, resulting in low seeding efficiency.[44] The CNF between the PCL

layers is likely to act as a hydrophilic physical barrier to the flow of the cell suspension through the pores, thus increasing the surface area and providing additional sites of adherence for the cells. Under similar conditions, electrospinning of collagen nanofibers between 3D printed PCL strands was reported to improve significantly the hydrophilicity, initial attachment and proliferation of osteoblast-like cells.[17, 18] Notably, the NaOH-etched surface alone showed no significant difference in the cell proliferation from the unmodified PCL scaffolds. In support of these findings, Kumar et al. reported that both solvent-etched and unmodified 3D printed PCL scaffolds support proliferation of hBMSCs without significant differences, up to 62 days.[41]

It is suggested that adhesion and spreading of mesenchymal stem cells occur in the first phase of cell-material interactions and influence the fate of the cells.[45] The hierarchical structure of scaffolds with micro-nanoscale features was reported to improve cell attachment, alignment, and spreading.[46] In the current study, SEM and AFM revealed that the CNF coating had a micro-nanoscale fibrillary structure. The microscale topography may dictate cell behavior by affecting whole cell morphology, while the nanoscale topography can interact with cellular sensing mechanisms such as filopodia and membrane receptors.[47] Filopodia are highly organized long bundles of actin filaments that have a role in cell adhesion.[46-48] Zhu et al. reported that smooth surfaces prevent extensions of osteoblastic filopodia, while on surfaces with micron and submicron roughness, cells developed strong anchorages.[48] In accordance with these reports, it is likely that the multiscale roughness of our CNF-coated scaffolds triggered the formation of cell anchorage filapodial extensions and offered favorable substrate for cell adhesion.

The adhesive capacity of the cells seeded onto CNF was confirmed by the production of vinculin protein, which regulates cell attachment-initiated signaling events.[49] Vinculin is known to be one of the focal adhesion molecules, involved not only in the connection between integrins

and the actin cytoskeleton, but also in the regulation of differentiation of mesenchymal stem cells via mechanotransduction.[50] The ability of CNF to stimulate the production of focal adhesion proteins could be attributable to the multiscale fibrillary structure as well as the surface chemistry.[51, 52] Surfaces with carboxylic groups were found to increase stem cell growth through up-regulation of focal adhesion components.[53] As the results of the present study showed that the physicochemical features of CNF enhanced protein adsorption, it is likely that proteins such as fibronectin and vitronectin in the adsorbed protein layer activated the focal adhesion pathway and increased the formation and organization of the actin cytoskeleton.[36] In addition, the shape and cytoskeleton organization of mesenchymal stem cells are known to dictate their fate by regulating different pathways such as the RhoA-ROCK signaling pathway.[41, 51, 54] Rounded cells tend to become adipocytes, while cells which spread tend to differentiate into osteoblasts.[54] The results showed that the cells cultured on CNF-coated surfaces adopted an elongated, well-spread morphology, which suggests their potential to differentiate towards osteoblasts.

The ability of CNF to differentiate hBMSCs was confirmed by the elevated ALP activity, mineral formation and collagen Type-I production. Alkaline phosphatase activity is known to be a prerequisite for the mineralization of the ECM and is closely associated with cellular differentiation.[15, 55] Moreover, the enhanced deposition of collagen Type I on CNF-coated TCP could explain the extensive formation of minerals, disclosed by Alizarin red S staining. It is well-known that the mineralization of bone ECM depends on the formation of a dense collagen Type I platform where calcium deposition can take place.[56] It is of interest to note that bone marrow mesenchymal cells from osteoporotic donors were found to produce an ECM deficient in Type I collagen, favoring adipogenic differentiation of cells.[57] This correlation between early (ALP) and

late (Alizarin red) mineralization of the collagen Type I matrix secreted by the cells are in agreement with other reports.[58, 59]

Generally, differentiation of mesenchymal stem cells is thought to be regulated by both physical and chemical cues, triggering different signaling pathways which guide the cells to different lineages.[51, 53, 54, 60] Kumar and colleagues suggested that the physical structure of scaffolds is more influential than chemical composition as determinants of differentiation of hBMSCs.[51] They showed that in the absence of osteogenic supplements, only polymeric scaffolds with nanofibrous morphology were able to drive the cells down the osteogenic lineage. Additionally, Khang et al. suggested that the nano-submicron roughness is influential in promoting osteoblast differentiation, initiating integrin activation and accelerating the expression of cyclins.[60] At the level of surface chemistry, Griffin et al. demonstrated that the introduction of carboxyl and amine groups to nanocomposite scaffolds regulates the differentiation of adipose stem cells towards osteogenic or chondrogenic lineages.[53] However, the cell-scaffold interaction is a complicated dynamic process and cannot be limited to the impact of a single individual surface feature.

It is of interest to note that the present results are in accordance with the few reports in the literature about the osteogenic potential of BNC, though some of these scaffolds were functionalized with osteogenic growth factors or nano-ceramics.[29, 30, 61] Moreover, the improved surface and biological properties of the PCL scaffolds in the current study are comparable to results obtained from other modification methods such as plasma treatment and protein immobilization.[15, 43] Plasma-treated 3D printed PCL scaffolds demonstrated enhanced cellular activities, mediated by improving the hydrophilicity and introducing nanoscale roughness to the surface. However, plasma treatment, unlike CNF coating, may suffer from aging that may happen over the storage, leading to changes to the modified surface of the polymers.[62]

Conclusions

Numerous studies have investigated different methods to enhance the osteogenic performance of 3D printed polymeric scaffolds. However, to date there are no studies reporting the use of CNF materials. The current study showed that, firstly, CNF significantly increased surface roughness, wettability and protein adsorption of PCL scaffolds. Secondly, the study demonstrated the ability of the CNF alone to maintain the viability, proliferation and differentiation of hBMSCs on CNF-coated tissue culture plates. CNF supported an elongated cell morphology and enhanced ALP activity, formation of collagen Type I and mineralization. Finally, the results showed superior cell-seeding efficiency on the CNF-coated 3D printed PCL scaffolds, and accordingly improved cellular attachment, proliferation and osteogenic differentiation. These findings suggest that wood-based nanocellulose, applied as a surface coating for open porous 3D printed scaffolds, can enhance hBMSCs differentiation *in vitro* and warrants evaluation in bone tissue regeneration *in vivo.*

Acknowledgements

This work has been funded by the Research Council of Norway through the NORCEL project, (Grant no. 228147) and Helse Vest projects 502027 and 912048. We would like to thank Ingebjørg Leirset, Odd J. Lundberg, Ying Xue and Mohamad Nageeb for their technical support.

Supporting Information

Mechanical characterization of PCL after NaOH treatment, micro-CT analysis of the 3D printed scaffolds after surface treatment, stability of the coating on the printed scaffolds, viability and morphology of hBMSCs cultured on CNF-coated surfaces, control immunostaining of collagen Type I and blank scaffolds after staining with Alizarin red S.

Disclosures

The authors declare that they have no conflicts of interest.

References

(1) Theocharis, A. D.; Skandalis, S. S.; Gialeli, C.; Karamanos, N. K., Extracellular matrix structure. *Adv. Drug Delivery Rev.* **2016,** 97, 4-27.

(2) Kim, D.-H.; Provenzano, P. P.; Smith, C. L.; Levchenko, A., Matrix nanotopography as a regulator of cell function. *J. Cell Biol.* **2012,** 197, (3), 351-360.

(3) O'Brien, C. M.; Holmes, B.; Faucett, S.; Zhang, L. G., Three-dimensional printing of nanomaterial scaffolds for complex tissue regeneration. *Tissue Eng., Part B.* **2015,** 21, (1), 103-14.

(4) Kang, H. W.; Lee, S. J.; Ko, I. K.; Kengla, C.; Yoo, J. J.; Atala, A., A 3D bioprinting system to produce human-scale tissue constructs with structural integrity. *Nat. Biotechnol.* **2016,** 34, (3), 312-9.

(5) Bose, S.; Vahabzadeh, S.; Bandyopadhyay, A., Bone tissue engineering using 3D printing. *Mater. Today* **2013,** 16, (12), 496-504.

(6) Jakus, A. E.; Rutz, A. L.; Jordan, S. W.; Kannan, A.; Mitchell, S. M.; Yun, C.; Koube, K. D.; Yoo, S. C.; Whiteley, H. E.; Richter, C. P.; Galiano, R. D.; Hsu, W. K.; Stock, S. R.; Hsu, E. L.; Shah, R. N., Hyperelastic "bone": A highly versatile, growth factor-free, osteoregenerative, scalable, and surgically friendly biomaterial. *Sci. Transl. Med.* **2016,** 8, (358).

(7) Saijo, H.; Igawa, K.; Kanno, Y.; Mori, Y.; Kondo, K.; Shimizu, K.; Suzuki, S.; Chikazu, D.; Iino, M.; Anzai, M.; Sasaki, N.; Chung, U. I.; Takato, T., Maxillofacial reconstruction using custom-made artificial bones fabricated by inkjet printing technology. *J. Artif. Organs* **2009,** 12, (3), 200-5.

(8) Hong, J. M.; Kim, B. J.; Shim, J. H.; Kang, K. S.; Kim, K. J.; Rhie, J. W.; Cha, H. J.; Cho, D. W., Enhancement of bone regeneration through facile surface functionalization of solid freeform fabrication-based three-dimensional scaffolds using mussel adhesive proteins. *Acta biomater.* **2012,** 8, (7), 2578-86.

(9) Yeong, W. Y.; Sudarmadji, N.; Yu, H. Y.; Chua, C. K.; Leong, K. F.; Venkatraman, S. S.; Boey, Y. C.; Tan, L. P., Porous polycaprolactone scaffold for cardiac tissue engineering fabricated by selective laser sintering. *Acta biomater.* **2010,** 6, (6), 2028-34.

(10) Pati, F.; Ha, D. H.; Jang, J.; Han, H. H.; Rhie, J. W.; Cho, D. W., Biomimetic 3D tissue printing for soft tissue regeneration. *Biomaterials* **2015,** 62, 164-75.

(11) Woodruff, M. A.; Hutmacher, D. W., The return of a forgotten polymer-Polycaprolactone in the 21st century. *Prog. Polym. Sci.* **2010,** 35, (10), 1217-1256.

(12) Olubamiji, A. D.; Izadifar, Z.; Si, J. L.; Cooper, D. M.; Eames, B. F.; Chen, D. X., Modulating mechanical behaviour of 3D-printed cartilage-mimetic PCL scaffolds: influence of molecular weight and pore geometry. *Biofabrication* **2016,** 8, (2), 025020.

(13) Lee, S. J.; Lee, D.; Yoon, T. R.; Kim, H. K.; Jo, H. H.; Park, J. S.; Lee, J. H.; Kim, W. D.; Kwon, I. K.; Park, S. A., Surface modification of 3D-printed porous scaffolds via mussel-

inspired polydopamine and effective immobilization of rhBMP-2 to promote osteogenic differentiation for bone tissue engineering. *Acta biomater.* **2016,** 40, 182-191.

(14) Uppanan, P.; Thavornyutikarn, B.; Kosorn, W.; Kaewkong, P.; Janvikul, W., Enhancement of chondrocyte proliferation, distribution, and functions within polycaprolactone scaffolds by surface treatments. *J. Biomed. Mater. Res., Part A* **2015,** 103, (7), 2322-32.

(15) Jeon, H.; Lee, H.; Kim, G., A surface-modified poly(varepsilon-caprolactone) scaffold comprising variable nanosized surface-roughness using a plasma treatment. *Tissue Eng., Part C.* **2014,** 20, (12), 951-63.

(16) Zhang, H.; Lin, C. Y.; Hollister, S. J., The interaction between bone marrow stromal cells and RGD-modified three-dimensional porous polycaprolactone scaffolds. *Biomaterials* **2009,** 30, (25), 4063-9.

(17) Yeo, M.; Lee, H.; Kim, G., Three-dimensional hierarchical composite scaffolds consisting of polycaprolactone, beta-tricalcium phosphate, and collagen nanofibers: fabrication, physical properties, and in vitro cell activity for bone tissue regeneration. *Biomacromolecules* **2011,** 12, (2), 502-10.

(18) Lee, H.; Yeo, M.; Ahn, S.; Kang, D. O.; Jang, C. H.; Lee, H.; Park, G. M.; Kim, G. H., Designed hybrid scaffolds consisting of polycaprolactone microstrands and electrospun collagen-nanofibers for bone tissue regeneration. *J. Biomed. Mater. Res., Part B* **2011,** 97, (2), 263-70.

(19) Ferreira, A. M.; Gentile, P.; Chiono, V.; Ciardelli, G., Collagen for bone tissue regeneration. *Acta biomater.* **2012,** 8, (9), 3191-200.

(20) Isogai, A.; Saito, T.; Fukuzumi, H., TEMPO-oxidized cellulose nanofibers. *Nanoscale* **2011,** 3, (1), 71-85.

(21) Lin, N.; Dufresne, A., Nanocellulose in biomedicine: Current status and future prospect. *Eur. Polym. J.* **2014,** 59, 302-325.

(22) Saito, T.; Okita, Y.; Nge, T. T.; Sugiyama, J.; Isogai, A., TEMPO-mediated oxidation of native cellulose: Microscopic analysis of fibrous fractions in the oxidized products. *Carbohydr. Polym.* **2006,** 65, (4), 435-440.

(23) Mertaniemi, H.; Escobedo-Lucea, C.; Sanz-Garcia, A.; Gandia, C.; Makitie, A.; Partanen, J.; Ikkala, O.; Yliperttula, M., Human stem cell decorated nanocellulose threads for biomedical applications. *Biomaterials* **2016,** 82, 208-20.

(24) Rashad, A.; Mustafa, K.; Heggset, E. B.; Syverud, K., Cytocompatibility of Wood-Derived Cellulose Nanofibril Hydrogels with Different Surface Chemistry. *Biomacromolecules* **2017,** 18, (4), 1238-1248.

(25) Lou, Y. R.; Kanninen, L.; Kuisma, T.; Niklander, J.; Noon, L. A.; Burks, D.; Urtti, A.; Yliperttula, M., The use of nanofibrillar cellulose hydrogel as a flexible three-dimensional model to culture human pluripotent stem cells. *Stem. Cells. Dev.* **2014,** 23, (4), 380-92.

(26) Bhattacharya, M.; Malinen, M. M.; Lauren, P.; Lou, Y. R.; Kuisma, S. W.; Kanninen, L.; Lille, M.; Corlu, A.; GuGuen-Guillouzo, C.; Ikkala, O.; Laukkanen, A.; Urtti, A.; Yliperttula, M., Nanofibrillar cellulose hydrogel promotes three-dimensional liver cell culture. *J. controlled release* **2012,** 164, (3), 291-8.

(27) Markstedt, K.; Mantas, A.; Tournier, I.; Martinez Avila, H.; Hagg, D.; Gatenholm, P., 3D Bioprinting Human Chondrocytes with Nanocellulose-Alginate Bioink for Cartilage Tissue Engineering Applications. *Biomacromolecules* **2015,** 16, (5), 1489-96.
(28) Mohamed-Ahmed, S.; Fristad, I.; Lie, S. A.; Suliman, S.; Mustafa, K.; Vindenes, H.; Idris, S. B., Adipose-derived and bone marrow mesenchymal stem cells: a donor-matched comparison. *Stem Cell Res. Ther.* **2018**, 9, (1), 168.
(29) Shi, Q.; Li, Y.; Sun, J.; Zhang, H.; Chen, L.; Chen, B.; Yang, H.; Wang, Z., The osteogenesis of bacterial cellulose scaffold loaded with bone morphogenetic protein-2. *Biomaterials* **2012,** 33, (28), 6644-9.
(30) Zang, S.; Zhuo, Q.; Chang, X.; Qiu, G.; Wu, Z.; Yang, G., Study of osteogenic differentiation of human adipose-derived stem cells (HASCs) on bacterial cellulose. *Carbohydr. Polym.* **2014,** 104, 158-65.
(31) Favi, P. M.; Benson, R. S.; Neilsen, N. R.; Hammonds, R. L.; Bates, C. C.; Stephens, C. P.; Dhar, M. S., Cell proliferation, viability, and in vitro differentiation of equine mesenchymal stem cells seeded on bacterial cellulose hydrogel scaffolds. *Mater. Sci. Eng. C* **2013,** 33, (4), 1935-44.
(32) Yeo, A.; Wong, W. J.; Khoo, H. H.; Teoh, S. H., Surface modification of PCL-TCP scaffolds improve interfacial mechanical interlock and enhance early bone formation: an in vitro and in vivo characterization. *J. of biomed. Mater. res. Part A* **2010,** 92, (1), 311-21.
(33) Sun, M.; Downes, S., Physicochemical characterisation of novel ultra-thin biodegradable scaffolds for peripheral nerve repair. *J. Mater. Sci.: Mater. Med.* **2009,** 20, (5), 1181-92.
(34) Thapa, A.; Webster, T. J.; Haberstroh, K. M., Polymers with nano-dimensional surface features enhance bladder smooth muscle cell adhesion. *J. Biomed. Mater. Res., Part A* **2003,** 67, (4), 1374-83.
(35) Arima, Y.; Iwata, H., Effect of wettability and surface functional groups on protein adsorption and cell adhesion using well-defined mixed self-assembled monolayers. *Biomaterials* **2007,** 28, (20), 3074-82.
(36) Yang, D.; Lü, X.; Hong, Y.; Xi, T.; Zhang, D., The molecular mechanism of mediation of adsorbed serum proteins to endothelial cells adhesion and growth on biomaterials. *Biomaterials* **2013,** 34, (23), 5747-5758.
(37) McClary, K. B.; Ugarova, T.; Grainger, D. W., Modulating fibroblast adhesion, spreading, and proliferation using self-assembled monolayer films of alkylthiolates on gold. *J. Biomed. Mater. Res.* **2000,** 50, (3), 428-39.
(38) Scopelliti, P. E.; Borgonovo, A.; Indrieri, M.; Giorgetti, L.; Bongiorno, G.; Carbone, R.; Podesta, A.; Milani, P., The effect of surface nanometre-scale morphology on protein adsorption. *PLoS One* **2010,** 5, (7), e11862.
(39) Isobe, N.; Lee, D.-S.; Kwon, Y.-J.; Kimura, S.; Kuga, S.; Wada, M.; Kim, U.-J., Immobilization of protein on cellulose hydrogel. *Cellulose* **2011,** 18, (5), 1251-1256.
(40) Gjerde, C.; Mustafa, K.; Hellem, S.; Rojewski, M.; Gjengedal, H.; Yassin, M. A.; Feng, X.; Skaale, S.; Berge, T.; Rosen, A.; Shi, X. Q.; Ahmed, A. B.; Gjertsen, B. T.; Schrezenmeier,

H.; Layrolle, P., Cell therapy induced regeneration of severely atrophied mandibular bone in a clinical trial. *Stem Cell Res. Ther.* **2018**, 9, (1), 213.
(41) Kumar, G.; Waters, M. S.; Farooque, T. M.; Young, M. F.; Simon, C. G., Jr., Freeform fabricated scaffolds with roughened struts that enhance both stem cell proliferation and differentiation by controlling cell shape. *Biomaterials* **2012,** 33, (16), 4022-30.
(42) Hua, K.; Rocha, I.; Zhang, P.; Gustafsson, S.; Ning, Y.; Stromme, M.; Mihranyan, A.; Ferraz, N., Transition from Bioinert to Bioactive Material by Tailoring the Biological Cell Response to Carboxylated Nanocellulose. *Biomacromolecules* **2016,** 17, (3), 1224-33.
(43) Alexandrescu, L.; Syverud, K.; Gatti, A.; Chinga-Carrasco, G., Cytotoxicity tests of cellulose nanofibril-based structures. *Cellulose* **2013,** 20, (4), 1765-1775.
(44) Declercq, H. A.; Desmet, T.; Berneel, E. E.; Dubruel, P.; Cornelissen, M. J., Synergistic effect of surface modification and scaffold design of bioplotted 3-D poly-epsilon-caprolactone scaffolds in osteogenic tissue engineering. *Acta biomater.* **2013,** 9, (8), 7699-708.
(45) Wang, Y. K.; Chen, C. S., Cell adhesion and mechanical stimulation in the regulation of mesenchymal stem cell differentiation. *J. Cell. Mol. Med.* **2013,** 17, (7), 823-32.
(46) Lopez-Bosque, M. J.; Tejeda-Montes, E.; Cazorla, M.; Linacero, J.; Atienza, Y.; Smith, K. H.; Llado, A.; Colombelli, J.; Engel, E.; Mata, A., Fabrication of hierarchical micro-nanotopographies for cell attachment studies. *Nanotechnology* **2013,** 24, (25), 255305.
(47) Albuschies, J.; Vogel, V., The role of filopodia in the recognition of nanotopographies. *Sci. Rep.* **2013,** 3, 1658.
(48) Zhu, X.; Chen, J.; Scheideler, L.; Altebaeumer, T.; Geis-Gerstorfer, J.; Kern, D., Cellular reactions of osteoblasts to micron- and submicron-scale porous structures of titanium surfaces. *Cells Tissues Organs* **2004,** 178, (1), 13-22.
(49) Carisey, A.; Ballestrem, C., Vinculin, an adapter protein in control of cell adhesion signalling. *Eur. J. Cell. Biol.* **2011,** 90, (2-3), 157-63.
(50) Holle, A. W.; Tang, X.; Vijayraghavan, D.; Vincent, L. G.; Fuhrmann, A.; Choi, Y. S.; del Alamo, J. C.; Engler, A. J., In situ mechanotransduction via vinculin regulates stem cell differentiation. *Stem Cells* **2013,** 31, (11), 2467-77.
(51) Kumar, G.; Tison, C. K.; Chatterjee, K.; Pine, P. S.; McDaniel, J. H.; Salit, M. L.; Young, M. F.; Simon, C. G., Jr., The determination of stem cell fate by 3D scaffold structures through the control of cell shape. *Biomaterials* **2011,** 32, (35), 9188-96.
(52) Faucheux, N.; Schweiss, R.; Lutzow, K.; Werner, C.; Groth, T., Self-assembled monolayers with different terminating groups as model substrates for cell adhesion studies. *Biomaterials* **2004,** 25, (14), 2721-30.
(53) Griffin, M. F.; Ibrahim, A.; Seifalian, A. M.; Butler, P. E. M.; Kalaskar, D. M.; Ferretti, P., Chemical group-dependent plasma polymerisation preferentially directs adipose stem cell differentiation towards osteogenic or chondrogenic lineages. *Acta biomater.* **2017,** 50, 450-461.

(54) Kilian, K. A.; Bugarija, B.; Lahn, B. T.; Mrksich, M., Geometric cues for directing the differentiation of mesenchymal stem cells. *Proc. Natl. Acad. Sci. U. S. A.* **2010,** 107, (11), 4872-7.
(55) Graneli, C.; Thorfve, A.; Ruetschi, U.; Brisby, H.; Thomsen, P.; Lindahl, A.; Karlsson, C., Novel markers of osteogenic and adipogenic differentiation of human bone marrow stromal cells identified using a quantitative proteomics approach. *Stem Cell Res.* **2014,** 12, (1), 153-65.
(56) Nudelman, F.; Pieterse, K.; George, A.; Bomans, P. H.; Friedrich, H.; Brylka, L. J.; Hilbers, P. A.; de With, G.; Sommerdijk, N. A., The role of collagen in bone apatite formation in the presence of hydroxyapatite nucleation inhibitors. *Nat. Mater.* **2010,** 9, (12), 1004-9.
(57) Rodriguez, J. P.; Montecinos, L.; Rios, S.; Reyes, P.; Martinez, J., Mesenchymal stem cells from osteoporotic patients produce a type I collagen-deficient extracellular matrix favoring adipogenic differentiation. *J. Cell. Biochem.* **2000,** 79, (4), 557-65.
(58) Ojansivu, M.; Vanhatupa, S.; Bjorkvik, L.; Hakkanen, H.; Kellomaki, M.; Autio, R.; Ihalainen, J. A.; Hupa, L.; Miettinen, S., Bioactive glass ions as strong enhancers of osteogenic differentiation in human adipose stem cells. *Acta biomater.* **2015,** 21, 190-203.
(59) Faia-Torres, A. B.; Charnley, M.; Goren, T.; Guimond-Lischer, S.; Rottmar, M.; Maniura-Weber, K.; Spencer, N. D.; Reis, R. L.; Textor, M.; Neves, N. M., Osteogenic differentiation of human mesenchymal stem cells in the absence of osteogenic supplements: A surface-roughness gradient study. *Acta biomater.* **2015,** 28, 64-75.
(60) Khang, D.; Choi, J.; Im, Y. M.; Kim, Y. J.; Jang, J. H.; Kang, S. S.; Nam, T. H.; Song, J.; Park, J. W., Role of subnano-, nano- and submicron-surface features on osteoblast differentiation of bone marrow mesenchymal stem cells. *Biomaterials* **2012,** 33, (26), 5997-6007.
(61) Fang, B.; Wan, Y. Z.; Tang, T. T.; Gao, C.; Dai, K. R., Proliferation and osteoblastic differentiation of human bone marrow stromal cells on hydroxyapatite/bacterial cellulose nanocomposite scaffolds. *Tissue Eng., Part A* **2009,** 15, (5), 1091-8.
(62) Siow, K. S.; Britcher, L.; Kumar, S.; Griesser, H. J., Plasma methods for the generation of chemically reactive surfaces for biomolecule immobilization and cell colonization - A review. *Plasma Process Polym.* **2006,** 3, (6-7), 392-418.

Graphical Abstract